

Elastic constants, phonon density of states, and thermal properties of UO₂M. Sanati,^{1,2,*} R. C. Albers,² T. Lookman,² and A. Saxena²¹*Physics Department, Texas Tech University, Lubbock, Texas 79409-1051, USA*²*Theoretical Division, Los Alamos National Laboratory, Los Alamos, New Mexico 89404, USA*

(Received 18 August 2010; revised manuscript received 26 April 2011; published 29 July 2011)

The elastic properties and phonon density of states of UO₂ have been studied by first-principles spin-polarized electronic-structure calculations in both the local density approximation (LDA) and the generalized-gradient approximation (GGA) for the experimentally determined antiferromagnetic spin configuration. Calculations have also been done both with and without Hubbard corrections (LDA + U and GGA + U). The elastic properties and phonon density of states are in very good agreement with experimental measurements when the Hubbard correction is included. The elastic constants and low-frequency (acoustic mode) phonons are in reasonably good agreement with experiment for all the different calculations. However, when Hubbard corrections are not included, the high-frequency phonons are pushed to lower frequencies and the optical phonons are significantly underestimated. The melting temperature is approximated by using an empirical equation, which uses elastic constants as input parameters, and is in good agreement with experiment. The first-principles calculations are also used to obtain the specific heat and entropy within the harmonic approximation at finite temperatures. It is shown that harmonic approximation is valid up to room temperature. The Debye temperature is estimated using two different methods. The predicted values are in excellent agreement with experimental results. It is shown that inclusion of the spin-orbit interaction does not significantly alter either the elastic or thermal properties.

DOI: [10.1103/PhysRevB.84.014116](https://doi.org/10.1103/PhysRevB.84.014116)

PACS number(s): 63.20.dk, 62.20.de

I. INTRODUCTION

Oxide fuels have received much experimental and theoretical attention because of their unique properties, such as high stability, melting temperature, fusion point, and the capacity to retain fission products.¹ For example, UO₂ is a commonly used fuel in pressurized heavy-water nuclear reactors. Understanding the physical, mechanical, and thermal properties of the fuel materials is primarily of interest in ensuring integrity of the core under operating conditions. Developing reliable theoretical modeling of such properties is a significant help, especially for the fuels without adequate experimental data such as PuO₂.

The elastic constants contain quite a bit of information about the stability and mechanical properties of solids. They are, for example, directly related to the bulk, shear, and Young's moduli. Also, the Debye temperature can be approximated by using the average speed of sound waves, which can be calculated from the elastic constants.² This is the easiest method for estimating this quantity, since it can be obtained either by experimental measurement or theoretical calculation. In addition, thermodynamic data such as the specific heat can also be used to determine the Debye temperature.

Based on experimental measurements of the elastic constants, Fritz³ reported a Debye temperature of 385 K for the UO₂ system, while with a similar approach Marlowe and Kaznoff⁴ found 875 K. Jones *et al.*⁵ reported a Debye temperature of 160 K obtained from low-temperature interpolation of their specific heat measurement. Dolling *et al.*⁶ have used the phonon density of states obtained from their neutron diffraction data in order to obtain the vibrational specific heat and to calculate the Debye temperature over a temperature interval between 0 and 500 K, with a zero-temperature value of 395 K. The enormous range of estimated or measured Debye temperatures strongly suggests that independent and

reliable modeling would be extremely useful for resolving this controversy.

First-principles band-structure calculations can provide valuable insight into physical, elastic, and thermal properties of materials. However, $5f$ -electron systems often have electronic correlation effects that cause the failure of conventional band-structure approaches such as the local density approximation (LDA) and generalized gradient approximation (GGA) to accurately predict many aspects of these materials. For example, such approaches predict a fluorite ($Fm\bar{3}m$) metallic ferromagnetic ground state for UO₂, while the observed ground state is an antiferromagnetic insulator with a band gap of about 2.0 eV.⁷ Several corrections to band theory that involve adding a Hubbard term to the Hamiltonian such as the DFT + U method^{8,9} and dynamical mean-field theory (DMFT),¹¹ and also some other first-principles approaches such as the GW quasiparticle method¹² and hybrid density-functional theory,¹³ do correctly predict the actual ground state for many materials, including UO₂ (note that GW approximations have not yet been performed on UO₂). However, the picture is muddled somewhat by the fact that some simple band-structure calculations on UO₂, such as for the lattice parameters and bulk modulus, appear less sensitive to the correlations effects and are in good agreement with experiment.

Since the elastic parameters are directly related to the low-frequency or acoustic phonons, it is not clear whether first-principles calculations with or without corrections would give a similar phonon density of states at all frequencies. The study of phonon spectra and lattice vibrations are of particular interest since many physical properties of crystals, including their specific heat, entropy, thermal expansion, thermal conductivity, phase transformations, melting, sound velocity, optical properties, and interaction with radiations such as x-ray and neutrons, are all related to the vibrations of the atoms in a solid. Therefore, it is essential to have a

reasonable phonon density of states for such an important material.

In this work we perform a systematic study of the elastic properties and phonon density of states of UO_2 within local spin density approximation (LSDA) and generalized gradient spin approximation (GGSA) with and without Hubbard corrections (in the LSDA + U and GGSA + U approximations) and spin-orbit interaction. Using the phonon density of states we have calculated the specific heat and entropy for different approximations within the harmonic approximation to the Helmholtz free energy. The specific heat at low temperatures as well as calculated elastic parameters are used to obtain the Debye temperature. This paper is organized as follows: Section II discusses the details of the methods used to perform the calculations. Section III contains the results and a discussion of the crystal parameters, elastic constants, bulk and shear moduli, phonon density of states, Debye temperature, specific heat, and entropy within the harmonic approximation. A summary of our main findings is presented in Sec. IV.

II. METHODOLOGY

Our electronic-structure calculations have been carried out using the first-principles density-functional pseudopotential package, VASP,^{14–16} within the local density (LDA) and generalized gradient approximation (GGA) to the exchange-correlation potential as parameterized by Perdew, Burke, and Ernzerhof (Ref. 17). In the VASP code we use the projector augmented-wave method^{18,19} with a cutoff kinetic energy of 500 eV. Since the experimentally observed magnetic structure for UO_2 is antiferromagnetic,^{20,21} all of the elastic and phonon properties that we present were calculated in a spin-polarized antiferromagnetic structure consistent with experiment. We have also done calculations including the Hubbard correction in the LDA + U or GGA + U approximation to approximately describe the correlated uranium f electrons, using the $U = 4.5$ eV and $J = 0.51$ eV values suggested by Dudarev *et al.*^{8,9} Since the elastic properties and phonons depend on the occupied electronic structure, changing the value of U mainly affects the size of the band gap and hence the unoccupied electronic structure. Probably any value of U that is large enough to open up a band gap would give similar or identical results. A few of our calculations also included the spin-orbit interaction in order to examine how strong an impact this had on the electronic structure. Spin-orbit (SO) calculations, of course, also require much longer computer runs. Electronic degrees of freedom were optimized with a conjugate gradient algorithm, and both cell constants and ionic positions were fully relaxed. The crystal was represented by 12 atom periodic cells. A modified tetrahedron method¹⁰ ($4 \times 4 \times 4$ mesh) was used for the k -point integration in the Brillouin zone. The elastic-constant, phonon, and thermodynamic methods are described below.

A. Elastic constants and melting temperature

There are three independent elastic constants for a lattice with cubic symmetry; C_{11} , C_{12} , and C_{44} . The elastic constant

C_{44} can be obtained from the following monoclinic volume conserving distortion,²²

$$\epsilon = \begin{pmatrix} 0 & \delta/2 & 0 \\ \delta/2 & 0 & 0 \\ 0 & 0 & \delta^2/(4 - \delta^2) \end{pmatrix},$$

where the energy increase (per unit cell volume) is given by:

$$E(\delta) = \frac{1}{2}C_{44}\delta^2 + O(\delta^4). \quad (1)$$

Similarly, the tetragonal shear constant C' [$C' = \frac{1}{2}(C_{11} - C_{12})$] can be obtained from the tetragonal volume conserving distortion,²²

$$\epsilon = \begin{bmatrix} \delta & 0 & 0 \\ 0 & -\delta & 0 \\ 0 & 0 & \delta^2/(1 - \delta^2) \end{bmatrix}.$$

The relation between the energy increase (per unit cell volume) and the distortion δ is given by

$$E(\delta) = 2C'\delta^2 + O(\delta^4). \quad (2)$$

The equilibrium volume (lattice constant) is obtained by fitting the total energy-volume data with Murnaghan's equation of state.²³ The bulk modulus for a cubic crystal is equal to $B = (C_{11} + 2C_{12})/3$ and can be obtained from the second derivative of the energy-volume curve. The C_{11} and C_{12} can be obtained from the calculated bulk modulus and C' .

The shear modulus G is obtained by solving the following Hershey-Kröner averaging method relation^{24,25} (see also the discussion in Refs. 26–28):

$$G^3 + \frac{9B + 4C'}{8}G^2 - \frac{3C_{44}(B + 4C')}{8}G - \frac{3BC_{44}C'}{4} = 0. \quad (3)$$

Another important mechanical parameter that is directly correlated to the ductility is the Poisson's ratio and given by

$$\nu = \frac{1}{2} \left(1 - \frac{E}{3B} \right), \quad (4)$$

where E is the Young's modulus and is related to the bulk and shear moduli:

$$E = \frac{9BG}{3B + G}. \quad (5)$$

The calculated lattice constant can also be used in order to estimate the melting temperature (T_m). Fine *et al.*²⁹ have studied many cubic metals and compounds and have obtained an approximate empirical linear relationship between T_m and the C_{11} elastic constant. The scatter of all the different points falls within plus or minus 300 K of the following equation for T_m in units of K:

$$T_m = 553 + \frac{5.91\text{K}}{\text{GPa}}C_{11}. \quad (6)$$

B. Debye temperature

Debye temperature is a very important parameter in solid-state physics and correlates with many physical and thermal properties of materials. There are many ways to approximate the Debye temperature for a system. In this work we used the calculated elastic constants in order to find the average of the sound velocities. The longitudinal and shear velocities are given by²:

$$v_l = \sqrt{(B + \frac{4}{3}G)/\rho}, \quad v_s = \sqrt{G/\rho}, \quad (7)$$

where ρ is the mass density of the material.

The Debye temperature θ_D is given by²

$$\theta_D = \frac{h}{k_B} \left[\frac{3}{4\pi} \left(\frac{N_A \rho}{M} \right) \right]^{\frac{1}{3}} \left[\frac{1}{3} \left(\frac{2}{v_s^3} + \frac{1}{v_l^3} \right) \right]^{-\frac{1}{3}}, \quad (8)$$

where h , k_B , N_A , and M , are Planck's constant, Boltzmann's constant, Avogadro's number, and average molecular weight, respectively.

C. Phonon and thermal calculations

The dynamical matrix calculations were performed using the force-constant method in 48-, 96-, and 192-atom cells with k -point sampling³⁰ of $3 \times 3 \times 2$, $2 \times 2 \times 2$, and $1 \times 1 \times 1$, respectively. The dynamical matrices are obtained from the Fourier transform of the force constant matrices. Diagonalization of the dynamical matrix yields the eigenfrequencies and eigenvectors.^{31,32} All of the force constants are calculated for the lattice constant with the minimum total energy (i.e., the lattice constants for each different method that are given in Table I).

The vibrational modes of the crystal are usually a much more important contribution to the free energy of the system than the electronic contribution. Significantly far below the melting point (when the anharmonicities get very severe), the vibrational free energy F_{vib} can be calculated within the harmonic approximation,³³

$$F_{\text{vib}}(T) = 3k_B T \int_{\Omega} \ln \left[2 \sinh \left(\frac{\hbar \omega}{2k_B T} \right) \right] g(\omega) d\omega, \quad (9)$$

where $g(\omega)$ is the phonon density of states. The vibrational entropy and specific heat at constant volume are calculated by

using the first and second derivatives of the Helmholtz free energy.³⁴

III. RESULTS AND DISCUSSION

A. Elastic properties and Debye temperature

The spin-polarized LDA (LSDA) and GGA (GGSA) calculations predict a metallic ferromagnetic fluorite structure. When the LSDA + U or GGSA + U have been used, like other published first-principles calculations, we found that the minimum energy crystal structure is an insulator fluorite structure. Depending on the choice of the U parameter one can find a 1- \mathbf{k} or 3- \mathbf{k} magnetic ordering for the ground state of this system.³⁵ Based on the parameters used in this work calculated ground state has 1- \mathbf{k} ordering with slightly distorted ($a = 5.4605 \text{ \AA}$, $c/a = 0.992$ with LSDA + U approximation) lattice constants relative to the cubic structure. However, in order to be consistent with the experimentally observed crystal structure (cubic) and because the theoretically predicted zero-temperature distortion is so small, we have done all of our elastic constant and phonon calculations for the cubic structure ($c/a = 1$). The LSDA + U method predicts a band gap of 1.9 eV and a magnetic moment of 1.851 Bohr magnetons on each uranium atom. The GGSA + U method gives a band gap of 2.1 eV and a uranium magnetic moment of 1.885 Bohr magnetons.

The lattice constants, elastic constants, bulk moduli, shear moduli, Young moduli, and Poisson's ratio for different approximations are given in Table I. The LSDA lattice constant is slightly too small. Both GGSA and GGSA + U tend to expand the lattice by a small amount. In general, the elastic constants and moduli obtained with LSDA + U and GGSA + U are in very good overall agreement with the measured values. As expected from the contracted lattice constant, the LSDA (without Hubbard U corrections) is in worst agreement of the various calculations. Overall, LSDA + U slightly overestimated elastic properties while GGSA + U underestimated them. Inclusion of the spin-orbit interaction did not improve the results significantly. It is interesting to note that GGSA still produces very accurate lattice and elastic parameters despite predicting the wrong type of ground state (ferromagnetic metal). This is likely because the elastic

TABLE I. Calculated lattice constant (a in \AA), elastic constants and bulk modulus (C_{ij} and B in GPa), pressure derivative of the bulk modulus (dB/dP , dimensionless), shear modulus and Young's modulus (G and E in GPa), Poisson's ratio (ν , dimensionless), and Debye temperature and melting temperature (θ and T_M in K) of UO_2 and the comparison of these quantities with experimental data.

	a (\AA)	C_{11} (GPa)	C_{12} (GPa)	C_{44} (GPa)	B (GPa)	dB/dP	G (GPa)	E (GPa)	ν	θ (K)	T_m (K)
LSDA	5.320	432.5	144.2	85.2	240.3	1.73	105.3	275.6	0.309	425	3109 ± 300
GGSA	5.423	367.0	114.7	62.9	198.8	4.34	83.3	219.3	0.316	390	2722 ± 300
LSDA + U	5.448	380.9	140.4	63.2	220.6	4.13	82.0	218.9	0.335	399	2804 ± 300
LSDA + U + SO	5.448	419.1	120.9	62.0	220.3	4.15	88.3	233.7	0.323	395	3030 ± 300
GGSA + U	5.548	345.7	115.5	63.4	192.2	4.21	80.6	212.1	0.316	388	2596 ± 300
Expt.	5.4731 ^a	389.3 ^b	118.7 ^b	59.7 ^b	209.0 ^b	4.69 ^b	83.0 ^b	221.0 ^b	0.324 ^b	385 ^b , 875 ^c	3120 ± 30^d

^aReference 36.

^bReference 3.

^cReference 4.

^dReference 38.

properties are relatively insensitive to the spin orientations and excited-state properties (the unoccupied states move higher in energy as the band gap is increased). As expected the GGSA with and without Hubbard corrections produces larger lattice constants and smaller bulk moduli with respect to the LSDA.

An LSDA + U calculation by Dudarev *et al.*⁹ has caused some controversy over the C_{44} elastic constant, since they found a rather large value (149 GPa) compared with the experimental value of 64 GPa. Kanchana *et al.*³⁷ suggested that this error might be caused by not relaxing the atomic positions of the anions (oxygen atoms). They performed first-principles LDA and GGA calculations on CeO₂, ThO₂, and PoO₂ fluorite-type structures and found for these materials that without such relaxation C_{44} was larger than the fully relaxed calculations by a factor of two. In all of the calculations reported in this work we have therefore fully relaxed the internal coordinates. Our calculations using LSDA + U and GGSA + U without any internal relaxation gave 71.7 and 67.2 GPa for C_{44} , respectively, whereas the fully relaxed values were 63.2 and 63.4 GPa (cf. Table I).

The C_{11} elastic constants obtained from the different approximations have been substituted into Eq. (6) in order to estimate the melting temperature for UO₂. As it can be seen from Table I, all of the approaches slightly underestimate the melting temperature with the LSDA, LSDA + U , and LSDA + U + SO being closest (between 2804 and 3109 K) to the experimental measurement³⁸ of 3120 K. Note, however, that LSDA and LSDA + U + SO overestimate C_{11} relative to the other approximations and experiment. A systematic study involving other actinide dioxides is needed to give us a better insight into the accuracy of Eq. (6) for predicting melting temperatures of mixed fuels.

The calculated elastic constants have been used to obtain the average longitudinal and shear velocities [see Eq. (7)]. From these quantities the Debye temperature can then be calculated from Eq. (8). A similar approach by Fritz³ gave 385 K for the Debye temperature and is in excellent agreement with our results. In agreement with Fritz³ we believe that the reported Debye temperature of 875 K by Marlow and Kaznoff⁴ must be caused by an algebraic mistake. Since the elastic data calculations are in good agreement with each other, this cannot be the source of such a huge error.

B. Phonon density of states

The elastic constants and the phonon dispersion (and hence phonon density of states) are directly related to each other (the elastic constants are proportional to the slopes of the linear low-frequency acoustic phonon modes that are linear in wave vector). Since we are using the direct method to calculate the phonons, it is important to test convergence in the size of the supercell used. Using the LSDA + U , the phonon densities for 48- and 96-atom cells are shown in Fig. 1. The phonon density of the 48-atom cell appears very similar to that of 96-atom cell, indicating good convergence for the vibrational and thermodynamical properties. Adding the spin-orbit interaction did not significantly modify the phonon density of states (Fig. 2) and, consequently, we did not consider this contribution for other results, since spin-orbit calculations drastically increase the computational expense of

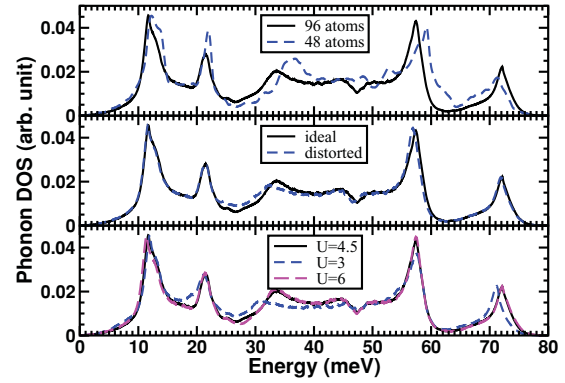


FIG. 1. (Color online) (Top) A comparison of the phonon density of states of 48- and 96-atom cells. (Middle) The phonon density of states of ideal and distorted 96-atom cells. (Bottom) The phonon density of states of the 96-atom cell for different values of the U parameter.

the calculations. Although the spin-orbit interaction has not improved the elastic properties of the system, it has significant effect on the electronic structure and local magnetization of the UO₂³⁹ and similar magnetic systems.⁴⁰

We have also checked the effect of the small theoretically predicted lattice distortion on the total phonon density of states of the system; this distortion was obtained by minimizing the total energy of the electronic structure calculations (see Sec. III A). Figure 1 shows the phonon density of states of the distorted and ideal 96-atom cells. It is obvious that the contribution of the lattice distortion is not significant. Another important question is the effect of the U parameter on the phonon density of states of the system. Figure 1 shows the phonon density of states for the different values of U when the exchange parameter J is kept constant. We found that phonon density of states converges for higher values of U . However in general, the different U values do not affect the phonon density of states significantly, which is consistent with the expectation that excited-state (unoccupied) properties of the electronic states should not affect ground-state materials properties very much.

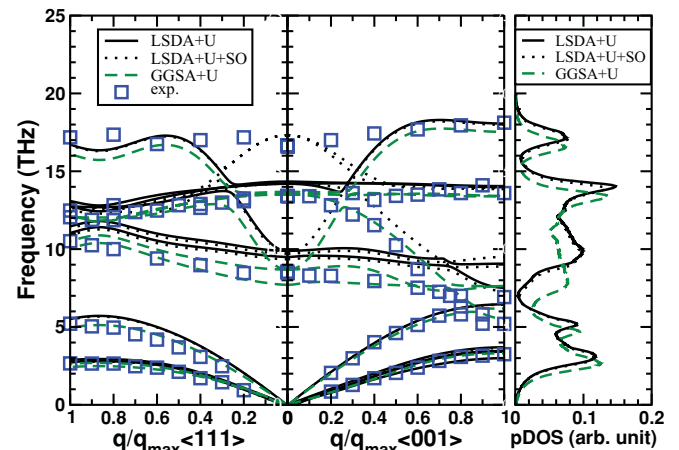


FIG. 2. (Color online) The phonon dispersion curves in two directions of high symmetry using a 192-atom cell. The experimental measurements⁶ are shown by the open symbols.

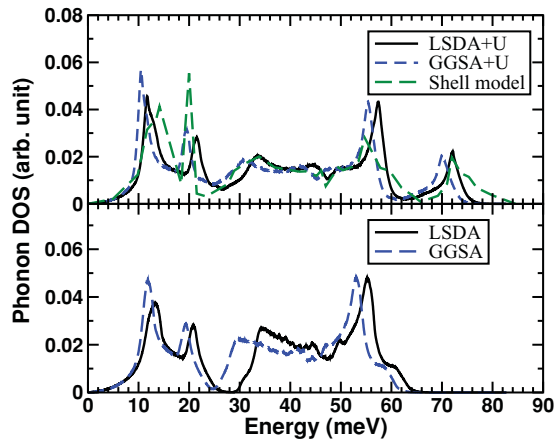


FIG. 3. (Color online) (Top) The phonon density of states obtained from LSDA + U , GGSA + U , and shell model.⁶ (Bottom) Calculated phonon density of states without Hubbard corrections.

A shell model of the dynamical matrix can be fitted to the experimental phonon dispersion curves in different directions.⁶ From the fitted phonon dynamical matrix, the “experimental” phonon density of states can be calculated. In Fig. 3 we compare our phonon density of states for the different approximations with the shell model. As can be seen from this figure, when Hubbard corrections are not included, the higher-frequency phonon modes are shifted to lower frequencies and the optical modes are underestimated. In addition, small band gaps in phonon densities of states around 24–30 meV are found for the LSDA and GGSA calculations that are not present for the other methods (or experiment). The calculated Γ -point optical phonon frequency for LSDA, GGSA, LSDA + U , and GGSA + U is 516 (63.9), 495 (61.4), 595 (73.8), and 579 (71.8) in units of cm^{-1} (meV), respectively, and can be directly compared to the measured value⁶ of $557 \pm 20 \text{ cm}^{-1}$ ($69.1 \pm 2.5 \text{ meV}$). Note that for the low-frequency phonon spectra (in the acoustic mode regime) the LSDA and GGSA phonon densities of states are very similar to that of LSDA + U and GGSA + U . At low temperatures the elastic properties and vibrational excitations are directly related to those modes. Therefore, LSDA and GGSA predict reasonably good elastic properties despite giving the wrong phonon density of states at higher frequencies.

In general we find a good overall agreement between phonon densities obtained from the (experimental) shell model and the LSDA + U and GGSA + U calculations, including the phonon density maxima and minima. However, there are some differences in the height of the peaks, especially around the 20 meV (4.8 THz) and 50 meV (12.1 THz) energy regions. Phonon densities of states from molecular dynamics simulations of UO_2 ,⁴¹ based on interatomic potential interactions, are similar to our calculations in that they also predict less sharp peaks. Note that calculated phonon dispersion curves along the high symmetry directions obtained in this work (Fig. 2) and molecular dynamics simulations are in very good agreement with experimental measurements for acoustic modes and optical modes around 4.8 and 12.1 THz, respectively. Thus, in addition to possible errors in the theoretical models, additional sources of discrepancies from the shell model could arise from approximations and errors in calculating the density of states

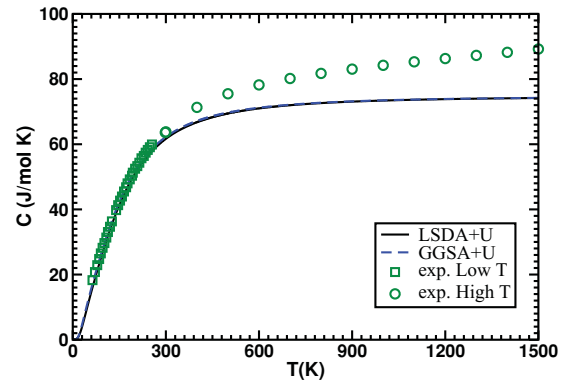


FIG. 4. (Color online) Calculated specific heat and its comparison with experimental measurements. The low- (open square) and high- (open circles) temperature data are taken from Refs. 5 and 42, respectively.

from phonons in the full Brillouin zone from a shell model that is only fit to a few high symmetry directions as well as from differences in temperature, since the phonon measurements were done at room temperature, whereas our calculations were performed at $T = 0 \text{ K}$. Note that there is a difference in the highest optical mode in both directions. However, considering the experimental estimated error⁶ of $\pm 1 \text{ THz}$ for these branches will result in a better agreement between the theory and experiment.

C. Specific heat and entropy

The phonon density of states has been used in order to calculate the specific heat and entropy of the system due to the vibrational modes. Since most experiments are conducted at constant pressure, it would be more relevant to calculate the Gibbs free energy. However, Helmholtz free energy has been calculated in this study instead. The results for specific heat and entropy and their comparison with experimental values are shown in Figs. 4 and 5, respectively. It is clear that the harmonic approximation gives reasonable values for specific heat up to the room temperature and after that there is a significant deviation from the measured values. Note that calculations without U approximation as well as GGSA

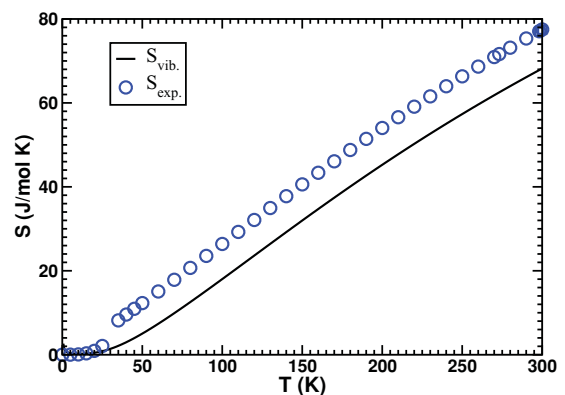


FIG. 5. (Color online) Calculated entropy and its comparison with experimental measurements. The values of entropy (open circle) are taken from Ref. 43.

give slightly higher specific heats. Since they underestimate the optical phonons, they have more lower frequency modes. These low-frequency modes have longer wavelengths and are associated with larger volumes in the configurational space. Therefore, they cause higher values for specific heat and entropy. It is instructive that for this system one should use the quasiharmonic approximation in order to have better results for the thermodynamical potentials.

In order to obtain another estimation of the Debye temperature we have fitted the calculated values of the specific heat between 8 and 18 K with the formula³³

$$C_v(T) = 9Nk_B \left(\frac{T}{\theta_D} \right)^3 \int_0^{\theta_D/T} \frac{x^4 e^x}{(e^x - 1)^2} dx, \quad (10)$$

(where $x = \frac{\hbar\omega}{k_B T} = \frac{\theta}{T}$) and interpolated the results to find θ_D at zero temperature.

This fitting results in predicted values of 405 and 391 K for LSDA + U and GGSA + U calculations, respectively. These temperatures are in excellent agreement with the temperature of 395 K, which has been obtained with a similar approach.⁶ The temperature of 160 K reported by Jones *et al.*⁵ is also not a reliable value since at 28.7 K there is an antiferromagnetic transformation in UO_2 . Thus, there is a magnetic contribution to the specific heat at low temperature that makes it difficult to estimate the Debye temperature with such a measurement. Based on our findings we believe that the Debye temperature of UO_2 should be around 400 K.

As can be seen from Table II, the specific heat and entropy at room temperature have been underestimated by 0.8–4.4% and 8.9–15.1% for 96-atom cell calculations. Since the entropy has been calculated by integration of the curve obtained from fitting the specific heats, one can ask this question: Why the entropy is underestimated by so much? The difference between entropies at room temperature and 35 K is given in Table II. The agreement between the calculated and experimental values

TABLE II. Calculated Γ phonon energy (in cm^{-1}) and the specific heat, entropy, and change in entropy (in J/mol K) at room temperature. The ΔS represents the difference between the entropy at room temperature and 35 K.

	Γ	C	S	ΔS
	(cm^{-1})	(J/mol K)	(J/mol K)	(J/mol K)
48-atom cell				
LSDA	484	62.82	68.86	66.61
GGSA	483	63.15	70.86	68.44
LSDA + U	599	60.60	64.65	62.65
LSDA + U + SO	596	61.71	69.75	66.72
GGSA + U	573	62.70	72.69	69.57
96-atom cell				
LSDA	516	62.1	66.66	64.66
GGSA	495	63.37	70.96	68.71
LSDA + U	595	61.11	66.15	64.35
GGSA + U	579	62.12	70.36	67.90
Expt.	557 ± 20^a	63.89^b	77.87^c	68.90^c

^aReference 6.

^bReference 5.

^cReference 43.

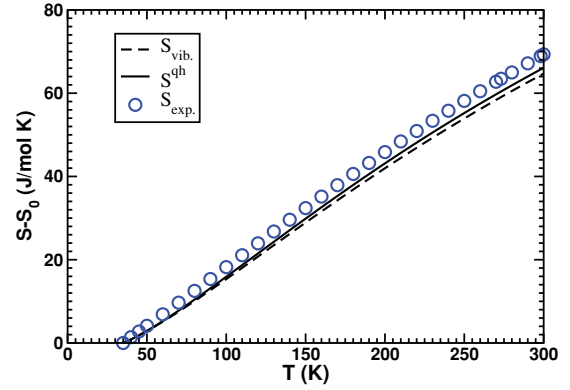


FIG. 6. (Color online) Calculated vibrational entropy difference with and without quasiharmonic approximation (solid line and dashed line) and its comparison with experimental measurements (open circles).⁴³ The S_0 is referred to the entropy at 35 K.

is much better than the abstract value at room temperature and the error (0.3–6.6%) is in the similar range of error for the specific heat. The plot of entropy difference versus temperature is depicted in Fig. 6. The agreement between experiment and prediction is much better than the absolute ones (Fig. 5). It looks like that part of the contribution to the entropy of the system has been neglected. As it can be seen from Fig. 5 around 30 K there is a jump in entropy of the system. After this temperature the entropy is almost parallel to the vibrational entropy of the system. This entropy increment is associated with the magnetic transition in the system. This contribution is usually evaluated by subtracting the lattice contribution from the measured entropy. However, in the UO_2 system the situation is more complex because of the coupled magnetic-lattice character of the transition. Therefore, if one subtracts the vibrational part of entropy, one obtains both magnetic and lattice contributions. In this case we can find an upper limit for the magnetic entropy. At 100 K, where the contribution from higher crystal field states should be negligible, we find an upper limit of 8.17 J/mol K. For a triple ground state one can expect an entropy contribution of $R \ln 3 = 9.1$ J/mol K^{5,6} which is in agreement with the predicted value.

Note that our calculations are performed within harmonic approximation that underestimates the entropy and specific heat at finite temperatures. In order to have some estimation about the finite temperature correction to harmonic approximation we used the following equation,

$$\frac{dS_{\text{vib}}^{\text{qh}}}{dT} = \frac{9Nk_B^2 \gamma^2}{BV_0}, \quad (11)$$

where γ , B , and V_0 are the average Gruneisen parameter, bulk modulus, and volume at 0 K, respectively. The input parameters are taken from experiment.³ At room temperature the correction to entropy due to thermal expansion is about 1.57 J/mol K. The entropy difference based on quasiharmonic approximation is shown in Fig. 6. There is slight improvement with respect to harmonic approximation at higher temperatures.

IV. SUMMARY

We have performed first-principles calculations to study the elastic and thermal properties of UO_2 . The lattice parameters, bulk, shear, and Young's moduli as well as Poisson's ratio for the fluorite phase are calculated. The phonon density of states of different approximations has been calculated. It was shown that the LSDA and GGSA without the Hubbard correction significantly underestimate the high-energy region of the phonon density of states (optical phonon). The effects of the Hubbard parameter (U) and size of the unit cell on phonon density of states have been investigated.

The vibrational free energy is obtained from first-principles calculations within the harmonic approximation. The specific heat at constant volume and entropy contribution to the free energy for all of the approximations are calculated. This approximation is valid up to room temperature. At higher temperatures one should calculate C_p instead of C_v .

The controversial Debye temperature (θ_D) was calculated by two different methods. In the first approach the elastic properties were used (we found Debye temperatures between 390 and 399 K except for the LDA method, which gave 425 K), and in the second approach this quantity was obtained by fitting to the specific heat at low temperatures (we found 405 and 391 K for LSDA + U and GGSA + U results). Calculated values from both methods are in excellent agreement with each other and close to the reported values of 385 and 395 K (Refs. 3 and 6).

ACKNOWLEDGMENTS

This work was carried out under the auspices of the National Nuclear Security Administration of the US Department of Energy at Los Alamos National Laboratory under Contract No. DE-AC52-06NA25396. We also acknowledge the generous amounts of computer time provided by Texas Tech University High Performance Computer Center.

*m.sanati@ttu.edu

¹C. Ronchi, I. L. Losilevski, and E. Yakub, *Equation of State of Uranium Dioxide* (Springer-Verlag, Berlin 2004).

²G. Grimvall, *Thermophysical Properties of Materials* (North-Holland, Amsterdam, 1999).

³I. J. Fritz, *J. Appl. Phys.* **47**, 4353 (1976).

⁴M. O. Marlowe and A. I. Kaznoff, in *Proceedings of the International Symposium on Nuclear Fuels* (American Ceramic Society, Westerville, Ohio, 1969), p. 90.

⁵W. M. Jones, J. Gordon, and E. A. Long, *J. Chem. Phys.* **20**, 695 (1952).

⁶G. Dolling, R. A. Cowley, and A. D. B. Woods, *Can. J. Phys.* **43**, 1397 (1965).

⁷Y. Baer and J. Schoenes, *Solid State Commun.* **33**, 885 (1980).

⁸S. L. Dudarev, D. Nguyen Manh, and A. P. Sutton, *Philos. Mag. B* **75**, 613 (1997).

⁹S. L. Dudarev, G. A. Botton, S. Y. Savrasov, Z. Szotek, W. M. Temmerman, and A. P. Sutton, *Phys. Status Solidi A* **166**, 429 (1998).

¹⁰P. E. Blöchl, O. Jepsen, and O. K. Andersen, *Phys. Rev. B* **49**, 16223 (1994).

¹¹S. Y. Savrasov, G. Kotliar, and E. Abrahams, *Nature (London)* **410**, 793 (2001).

¹²W. G. Aulbur, L. Jonsson, and J. W. Wilkins, *Solid State Phys.* **54**, 1 (2000).

¹³K. N. Kudin, G. E. Scuseria, and R. L. Martin, *Phys. Rev. Lett.* **89**, 266402 (2002).

¹⁴VASP at [<http://cms.mpi.univie.ac.at/vasp>].

¹⁵G. Kresse and J. Hafner, *Phys. Rev. B* **47**, 558 (1993).

¹⁶G. Kresse and J. Furthmüller, *Phys. Rev. B* **54**, 11169 (1996).

¹⁷J. P. Perdew, K. Burke, and M. Ernzerhof, *Phys. Rev. Lett.* **77**, 3865 (1996).

¹⁸P. E. Blöchl, *Phys. Rev. B* **50**, 17953 (1994).

¹⁹G. Kresse and D. Joubert, *Phys. Rev. B* **59**, 1758 (1999).

²⁰J. Faber, G. H. Lander, and B. R. Cooper, *Phys. Rev. Lett.* **35**, 1770 (1975).

²¹J. Faber and G. H. Lander, *Phys. Rev. B* **14**, 1151 (1976).

²²M. J. Mehl, J. E. Osburn, D. A. Papaconstantopoulos, and B. M. Klein, *Phys. Rev. B* **41**, 10311 (1990).

²³F. D. Murnaghan, *Proc. Natl. Acad. Sci. USA* **30**, 244 (1944).

²⁴A. V. Hershey, *J. Appl. Mech. Trans. ASME* **21**, 236 (1954).

²⁵E. Kröner, *Z. Phys.* **151**, 504 (1958).

²⁶H. M. Ledbetter, *J. Appl. Phys.* **44**, 1451 (1973).

²⁷H. M. Ledbetter, *J. Phys. D* **13**, 1879 (1980).

²⁸H. M. Ledbetter, *Phys. Status Solidi A* **85**, 89 (1984).

²⁹M. E. Fine, L. D. Brown, and H. L. Marcus, *Scr. Metall.* **18**, 951 (1984).

³⁰H. J. Monkhorst and J. D. Pack, *Phys. Rev. B* **13**, 5188 (1976).

³¹M. Sanati, D. West, and R. C. Albers, *J. Phys. Condens. Matter* **19**, 386221 (2007).

³²M. Sanati, D. West, and R. C. Albers, *J. Phys. Condens. Matter* **20**, 465206 (2008).

³³A. A. Maradudin, E. W. Montroll, G. H. Weiss, and I. P. Ipatova, *Theory of Lattice Dynamics in the Harmonic Approximation* (Academic Press, New York, 1971).

³⁴M. Sanati and S. K. Estreicher, *J. Phys. Condens. Matter* **16**, L327 (2004).

³⁵R. Laskowski, G. K. H. Madsen, P. Blaha, and K. Schwarz, *Phys. Rev. B* **69**, 140408 (2004).

³⁶M. Idiri, T. Le Bihan, S. Heathman, and J. Rebizant, *Phys. Rev. B* **70**, 014113 (2004).

³⁷V. Kanchana, G. Vaitheeswaran, A. Svane, and A. Delin, *J. Phys. Condens. Matter* **18**, 9615 (2006).

³⁸M. G. Adamson, E. A. Aitken, and R. W. Caputi, *J. Nucl. Mater.* **130**, 349 (1985).

³⁹S. L. Dudarev, M. R. Castell, G. A. Botton, S. Y. Savrasov, C. Muggelberg, G. A. D. Briggs, A. P. Sutton, and D. T. Goddard, *Micron* **31**, 363 (2000).

⁴⁰M. R. Castell, S. L. Dudarev, G. A. D. Briggs, and A. P. Sutton, *Phys. Rev. B* **59**, 7342 (1999).

⁴¹P. Goel, N. Choudhury, and S. L. Chaplot, *J. Nucl. Mater.* **377**, 438 (2008).

⁴²G. E. Moore and K. K. Kelley, *J. Amer. Chem. Soc.* **69**, 2105 (1947).

⁴³J. J. Huntzicker and E. F. Westrum Jr., *J. Chem. Thermodyn.* **3**, 61 (1971).